Event-Related fMRI Contrast When Using Constant Interstimulus Interval: Theory and Experiment

Peter A. Bandettini* and Robert W. Cox

Event-related functional magnetic resonance imaging (ER-fMRI) involves the mapping of averaged hemodynamic changes resulting from repeated, brief (<3 sec) brain activation episodes. In this paper, two issues regarding constant-interstimulus interval ER-fMRI were addressed. First, the optimal interstimulus interval (ISI), given a stimulus duration (SD), was determined. Second, the statistical power of ER-fMRI relative to that of a blocked-design paradigm was determined. Experimentally, it was found that with a 2-sec SD, the optimal ISI is 12 to 14 sec. Theoretically, the optimal repetition interval (T_{opt} = ISI + SD) is 12 to 14 sec for stimuli of 2 sec or less. For longer stimuli, T_{opt} is $8 + 2 \cdot$ SD. At the optimal ISI for SD = 2 sec, the experimentally determined functional contrast of ER-fMRI was only −35% lower than that of blocked-design fMRI. Simulations that assumed a linear system demonstrated an event-related functional contrast that was −65% lower than that of the blocked design. These differences between simulated and experimental contrast suggest that the ER-fMRI amplitude is greater than that predicted by a linear shift-invariant system. Magn Reson Med 43:540–548, 2000. © 2000 Wiley-Liss, Inc.
Key words: human brain mapping; fMRI; BOLD; event-related

Brain activation causes highly localized and time-locked changes in blood flow, volume, and oxygenation. These changes are detectable using functional magnetic resonance imaging (fMRI) (1–5). The most commonly used fMRI pulse sequences are those that are sensitized to localized susceptibility changes that accompany changes in blood oxygenation. This type of contrast was coined blood oxygenation level dependent (BOLD) contrast by Ogawa et al. (6). On activation, the time for the BOLD response to first significantly increase from baseline is approximately 2 sec (7,8). The time to plateau in the "on" state is approximately 6 to 9 sec (7). On cessation of activation, the time to return to baseline is longer than the rise time by about 1 sec (9).

Deconvolution of a neuronal input function from the measured hemodynamic response gives a hemodynamic "impulse response" that roughly resembles the type of response that is induced by a brief stimulus (10). To draw precise inferences from this analysis, it is necessary to assume that the hemodynamic response behaves like a linear system. Issues related to the linearity of the hemodynamic response have been addressed (11–15). Boynton et al. (12) and Vazquez and Noll (15) have presented results suggesting a nonlinearity of the hemodynamic re-

sponse during brief (<4 sec) stimulus durations. Dale and Buckner (14) give evidence that the responses from brief stimuli presented in rapid succession add in an approximately linear manner. These issues are discussed in the context of the results presented. (In this paper, "linearity" refers to the assumption that the transformation between the stimulus time series and a voxel response time series—two observables—is a linear one.)

Event-related experiments involving brief periods of sensory and motor activation demonstrated that the hemodynamic response peaks at about 5 to 6 sec, then returns to baseline at about 10 sec (9,14,16–20). The onset is sometimes preceded by a "pre-undershoot," (21–23). The return to baseline is sometimes followed by a "post-undershoot" (5,24–27). The post-undershoot is larger in magnitude and more commonly observed than the pre-undershoot. Basic concepts regarding event-related hemodynamic response characteristics and analysis have been published (12–15,28,29). Recently, "event-related" activation strategies have become more extensively characterized and applied in the context of cognitive experiments (20,30–34).

There are many advantages of event-related activation strategies (34), including more complete randomization of task types in a time series (14,31,32), selective analyses of fMRI response data based on measured behavioral responses to individual trials (33), and separation of motion artifact due to overt responses from BOLD changes by use of temporal response differences between motion effects and BOLD contrast-based changes (35,36).

A time series of multiple, sequential single-event brain activation tasks or stimuli can be thought to involve two primary variables: the stimulus duration (SD) and the interstimulus interval (ISI). Event-related studies reported in the literature have employed SDs that vary from 0.33 sec to 2 sec, and ISIs that vary from 30 sec to 2 sec.

Event-related experimental design strategies can be divided into two categories The first involves randomization of the ISI during a time series and subsequent deconvolution of the "impulse response." Analysis of this impulse response uses the assumption that the hemodynamic response is linear system. Processing issues related to this assumption are outside the scope of this paper. The second strategy involves the use of a constant ISI. While constant ISI strategies may be less time efficient than randomized ISI strategies, analysis of constant ISI ER-fMRI is straightforward, involving simple binning and averaging. No deconvolution is necessary and therefore no assumptions of linearity are necessary. A primary focus of this paper is the optimization of constant ISI strategies.

Two questions arise when considering the design of an ER-fMRI experiment using a constant ISI. The first is, "What is the optimum ISI for a given SD?" For many cognitive experiments, the SD is roughly 1 to 2 sec—the

Biophysics Research Institute, Medical College of Wisconsin, Milwaukee, Wisconsin.

*Correspondence to: Peter A. Bandettini, Ph.D., NIH, National Institute of Mental Health, Laboratory of Brain and Cognition, Building 10, Room 4C104, 10 Center Dr. MSC 1366, Bethesda, MD 20892-1366.
E-mail: bandettini@nih.gov

average time necessary to fully perform the individual task. More trials per unit time tend to increase the statistical power, but the slowness of the hemodynamic response causes significant signal overlap if the trials are spaced too closely in time. This overlap can cause saturation of the fMRI signal (usually indicated by an increase in the baseline level) and subsequently attenuation of the amplitude or reduction of the available dynamic range of the event-related responses ("clipping" of the fMRI responses). The attenuation in amplitude change decreases the ability to detect the fMRI response and the statistical power of its amplitude estimate. The tradeoff is therefore between the number of trials per unit time and the degree of attenuation of the event-related response that occurs with close temporal spacing. This tradeoff depends on the shape and latency of the impulse response. The second question regards how the statistical power of ER-fMRI compares with fMRI using more conventional blocked designs (i.e., repeated cycles of ≈20 sec "on" and ≈20 sec "off"). This is an important consideration when deciding on the duration and number of time series that are necessary for a study. The work in this paper, presented in preliminary abstract form (37–39), addresses these two questions theoretically and experimentally.

THEORY

We assume that the MR signal response is given by a linear shift-invariant filter applied to the underlying "activity" in each voxel. (The history-dependent nonlinearity in fMRI signals discussed recently by Friston et al. (13) is not considered in this analysis.) The response function of this filter to a single stimulus is denoted by $r(t)$. We assume throughout that the noise, ζ, is stationary and white, with variance σ^2. We assume that a single stimulus is repeated periodically. The goal is to estimate accurately the response magnitude in each voxel time series. Our signal model in each voxel, expressed in continuous and discrete time, is

$$x(t) = \alpha \sum_{m=0}^{M-1} r(t - mT) + \beta + \zeta(t) \qquad [1a]$$

$$x_n = \alpha \sum_{m}^{m=0} r_{n-mL} + \beta + \zeta_n \qquad [1b]$$

$$\mathbf{x} = [\mathbf{r}^{(L)} \mathbf{e}_N] \begin{bmatrix} \alpha \\ \beta \end{bmatrix} + \zeta \qquad [1c]$$

where α is the response magnitude, β is the signal baseline, and $x_n = x(n\Delta t)$ is the voxel signal at the nth sample (expressed in vector form in Eq. [1c]). The N-vector $\mathbf{r}^{(L)}$ is defined by $r_n^{(L)} = \sum_m r_{n-Lm}$; the N-vector $\mathbf{e}_N$ is all ones. The goal is to estimate α but β is also unknown. The estimate of α depends on the repetition period $T = L\Delta t = \text{SD} + \text{ISI}$ and on the number of trials M. The total length of the experiment is $ML\Delta t = N\Delta t$.

Define $\mathbf{P}$ to be the $N \times 2$ matrix appearing in the RHS of Eq. [1c] ($p_{n,1} = r_n^{(L)}$ and $p_{n,2} = 1$). Then the minimum variance linear unbiased estimator of α and β is given by

$$\begin{bmatrix} \hat{\alpha} \\ \hat{\beta} \end{bmatrix} = [\mathbf{P}^*\mathbf{P}]^{-1}\mathbf{P}^*\mathbf{x} \quad \text{Cov}\begin{bmatrix} \hat{\alpha} \\ \hat{\beta} \end{bmatrix} = \sigma^2[\mathbf{P}^*\mathbf{P}]^{-1} \qquad [2a]$$

$$\mathbf{P}^*\mathbf{P} = \begin{bmatrix} \sum_n (r_n^{(L)})^2 & \sum_n r_n^{(L)} \\ \sum_n r_n^{(L)} & N \end{bmatrix} \quad \text{Var}(\hat{\alpha})$$

$$= \frac{N\sigma^2}{N \sum_n (r_n^{(L)})^2 - (\sum_n r_n^{(L)})^2}. \qquad [2b]$$

If the stimuli are spaced far enough apart so that the responses do not significantly overlap, then $r^{(L)} = r_{n-[n/L]L}$, so

$$\sum_n r_n^{(L)} = M \sum_{n=0}^{L-1} r_n \approx M\Delta t^{-1}\mu_1 \quad \sum_n (r_n^{(L)})^2 = M \sum_{n=0}^{L-1} r_n^2$$

$$\approx M\Delta t^{-1}\mu_2 \qquad [3]$$

where $\mu_q = \int_o^o r(t)^q dt$. These integral approximations are valid if Δt is small compared to the rise and fall times of the response function.

We want to minimize $\text{Var}(\hat{\alpha})$ for a fixed amount of scan time $N\Delta t$ by properly choosing the stimulation period $L\Delta t$. We can write $M = N/L$, and then

$$\frac{1}{\text{Var}(\hat{\alpha})} \approx \frac{1}{N\sigma^2}(N^2 L^{-1}\Delta t^{-1}\mu_2 - N^2 L^{-2}\Delta t^{-2}\mu_1^2)$$

$$= \frac{N}{\sigma^2} \cdot \frac{1}{L\Delta t}\left(\mu_2 - \frac{1}{L\Delta t}\mu_1^2\right). \qquad [4]$$

Optimizing Eq. [4] with respect to $T = L\Delta t$, we find

$$T_{\text{opt}} = 2\frac{\mu_1^2}{\mu_2} = 2\frac{\left(\int r(t)\, dt\right)^2}{\int r(t)^2\, dt}. \qquad [5]$$

This is equivalent to maximizing the expected value of $\int |x(t) - \bar{x}|^2 dt$, which shows that the optimum stimulus period is based on balancing the time budget between the stimulus response and the baseline state.

Theoretical Examples

The simplest response function is a "boxcar" of duration τ:

$$r_{\text{box}} = \begin{cases} 1 & 0 < t < \tau \\ 0 & \text{otherwise.} \end{cases}$$

In this case, $\mu_1 = \mu_2 = \tau$, and so $T_{\text{opt}} = 2\tau$; that is, equal times should be spent in the stimulus response and in the

baseline. A slightly more realistic response function is the triangle wave with rise/fall time τ:

$$r_{\text{tri}} = \begin{cases} 1 - |t - \tau|/\tau & 0 < t < 2\tau \\ 0 & \text{otherwise.} \end{cases}$$

In this case, $\mu_1 = \tau$, and $\mu_2 = 2\tau/3$, so $T_{\text{opt}} = 3\tau = 3 \cdot$ FWHM (full width at half maximum of the response function). In this case, the optimal balance is to spend 1/3 the time in the baseline and 2/3 in the stimulus response. For fMRI, a reasonable estimate of the rise/fall time is $\tau \approx 5$ sec, giving $T_{\text{opt}} \approx 15$ sec. For the gamma-variate impulse response function (28),

$$r_\Gamma(t;b,c) = \begin{cases} t^b e^{-t/c} & t > 0 \\ 0 & t < 0 \end{cases} \quad \text{we find} \quad T_{\text{opt}} = \frac{2b4^b \Gamma(b)^2}{\Gamma(2b)} \cdot c.$$

[6]

Realistic values for fMRI are $b = 8.6$, $c = 0.55$ sec, giving $T_{\text{opt}} = 11.6$ sec. If the SD is extended to 2 sec, then with $r(t) = r_{\text{box}}(t,2) * r_\Gamma(t;8.6,0.55)$, $T_{\text{opt}} = 12.3$ sec (here, "$*$" denotes convolution). For general parameters b, c in Eq. [6], the time-to-peak is $t_{\text{peak}} = bc$; the width of the response function is FWHM $\approx 2.35 \cdot b^{1/2}c$, and $T_{\text{opt}} \approx 7.09 \cdot b^{1/2}c \approx 3 \cdot$ FWHM. (These latter two approximations are valid for $b \geq 2$.)

As our final mathematical result, we note that for longer duration stimuli, 2 sec should be added to T for each additional 1 sec of stimulation. We base this on the observation that if $r(t) = r_{\text{box}}(t;\tau) * r_{\text{box}}(t;SD)$, with $\tau > SD$ (a trapezoidal waveform), then $T_{\text{opt}} = 2 \cdot SD^2/(SD - \tau/3)$, which is asymptotic to $2 \cdot SD + 2\tau/3$ for $SD \gg \tau$. That is, for large SD, the optimal period T increases twice as fast as SD; the increased time in the "on" phase must be balanced by additional "off" time. In our linear model, for any given impulse response function $r(t)$, the response to a stimulus of duration SD is $r(t) = r(t) * r_{\text{box}}(t;SD)$. For large SD, this function will have a long flat top with smooth transitions at the beginning and end (a rounded trapezoid) for which we have seen that T_{opt} grows like $2 \cdot SD$ for SD larger than the rise and fall times of the impulse response. Figure 1 shows a graph of T_{opt} versus SD for the gamma-variate impulse response function, where $r(t) = r_\Gamma(t;8.6,0.55) * r_{\text{box}}(t;SD)$.

Based on this, our ultimate theoretical recommendation is

$$\text{ISI} = \begin{cases} 14 - SD & SD < 3 \text{ s} \\ 8 + SD & SD > 3 \text{ s} \end{cases} \quad \text{or} \quad T$$

$$= \begin{cases} 14 & SD < 3 \text{ s} \\ 14 + 2 \cdot (SD - 3) & SD > 3 \text{ s} \end{cases}. \quad [7]$$

Note that the commonly used block-design choice of ISI = SD is slightly too small. It is important to note that the optimal T will vary also as a function of the gamma variate parameters. Unpublished data in our lab clearly indicate that these parameters vary over space. This issue is beyond the scope of this paper. This contrast function obtained in Fig. 1 is simply an approximate guideline based on a reasonable estimate of the response.
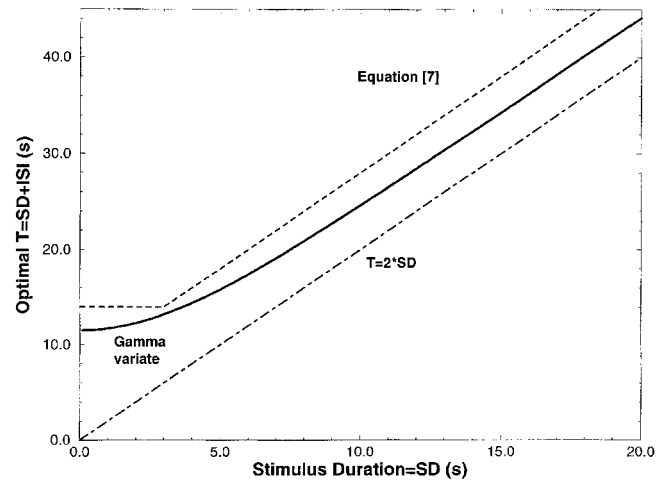

FIG. 1. Graph of optimal $T = SD + ISI$ versus SD when the hemodynamic response is modeled as the gamma-variate function convolved with a boxcar of duration SD (T_{opt} was computed numerically from Eq. [5]). Shown for comparison are the graphs of $T = 2 \cdot SD$ and the recommendation of Eq. [7].

METHODS

Five subjects were scanned with echoplanar imaging (EPI) using a three-axis gradient coil (40) on a GE Signa 1.5-T scanner. Results from two subjects were discarded because of significant motion artifacts. Two axial imaging planes were obtained: one containing visual cortex and one containing motor cortex. Acquisition parameters were: voxel volume = $3.7 \times 3.7 \times 7$ mm^3, TR = 1 sec, TE = 40 msec, and time series length = 360 images. Flashing 8-Hz red LED visual stimulation was given using GRASS goggles. Subjects performed bilateral finger tapping while the visual stimulus was on. We chose 2 sec as the SD since, in the context of a cognitive experiment, the total task completion time can be as high as 2 sec. For two subjects, separate time series with ISIs of 2, 4, 6, 8 10, and 12 sec were collected. For one subject, separate time series with ISIs of 6, 8, 10, 16, 20, and 24 sec were collected. A "blocked" time series having timing of 20 sec on/20 sec off was also collected for all subjects. Table 1 summarizes the

Table 1
Summary of the Experimental Comparisons*

ISI (sec)	SD (sec)	# Cycles
20	20	9
24	2	13
20	2	16
16	2	20
12	2	25
10	2	30
8	2	36
6	2	45
4	2	60
2	2	90

*Time series length = 360 images. TR = 1 sec. For the event-related design, SD = 2 sec, and ISI is varied from 2 sec to 20 sec. The blocked design is 20 sec on/20 sec off.

FIG. 2. Typical echoplanar images from the time series data. Superimposed in white are the visual and motor cortex voxels that demonstrated activation. The time series in Fig. 3 were averaged over these ROIs. Activated voxels were determined by correlation analysis using a time-shifted boxcar function with the blocked-design time series.
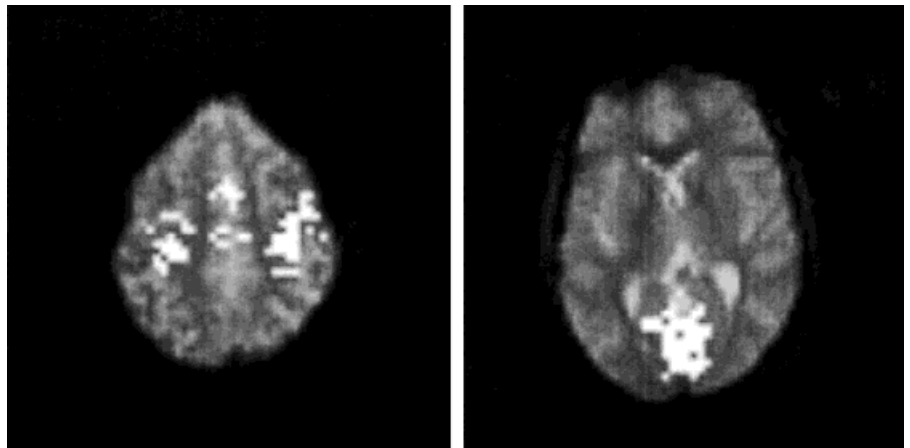
experimental design. The time series order, and therefore ISI order, was randomized for each subject.

From the experimental time series, both functional contrast-to-noise images and response curves were analyzed. Functional contrast-to-noise images were created in the following manner. First, an activated region of interest (ROI) was determined from the "blocked" time series by correlation analysis with a time-shifted boxcar function (41). Second, from this ROI, average plots were obtained for each time series of images. Third, using these time plots, a reference function was synthesized by first averaging every on/off cycle, then sequentially replicating the average cycle for the entire time plot. Fourth, a correlation image was created using each of the synthesized reference functions (one reference function for each ISI). Finally, the calculated correlation image was divided by the residual time series standard deviation (after subtracting away the reference function) on a voxel-wise basis to create a functional contrast-to-noise image. Using the ROI determined by step one above, the average contrast-to-noise value was obtained from each contrast-to-noise image.

A second method for assessing functional contrast involved calculating the integral of the rectified area around the mean of averaged responses (obtained from the same ROI for motor and visual cortex as used above). This integral was divided by the time per complete event-related on/off cycle to obtain a measure of contrast per unit time.

For the simulations, response waveforms were created by convolving the gamma-variate hemodynamic response function described earlier with binary on/off functions that represent the neuronal input. The contrast per unit time was calculated in these synthesized responses in the same manner as with the experimentally obtained response curves: the integral of the rectified area around the mean of curves was divided by the total stimulus cycle time, T.

RESULTS

Figure 2 shows typical echoplanar images obtained and, superimposed in white, visual and motor cortex regions that demonstrated activation. Time series obtained from these ROIs are shown in Fig. 3. Each time series plot in Fig. 3 is displayed having identical dynamic range. In each
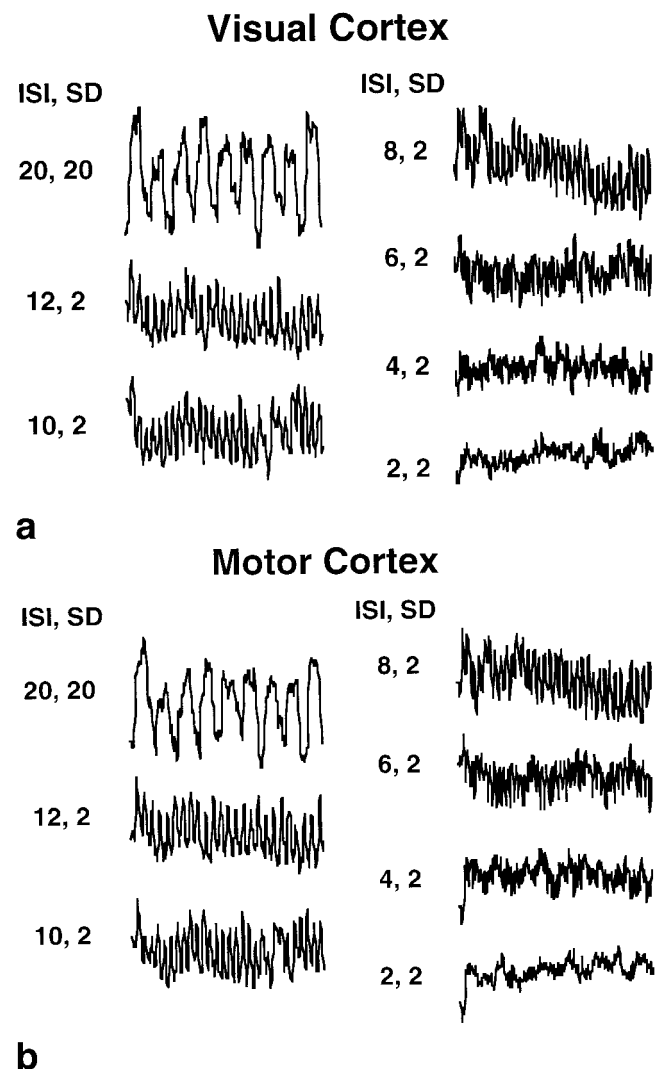

FIG. 3. Raw time series from the (**a**) visual and (**b**) motor ROIs in Fig. 2. The blocked-design paradigm time series is in the upper left. SD is varied from 12 to 2 sec for the other time series.
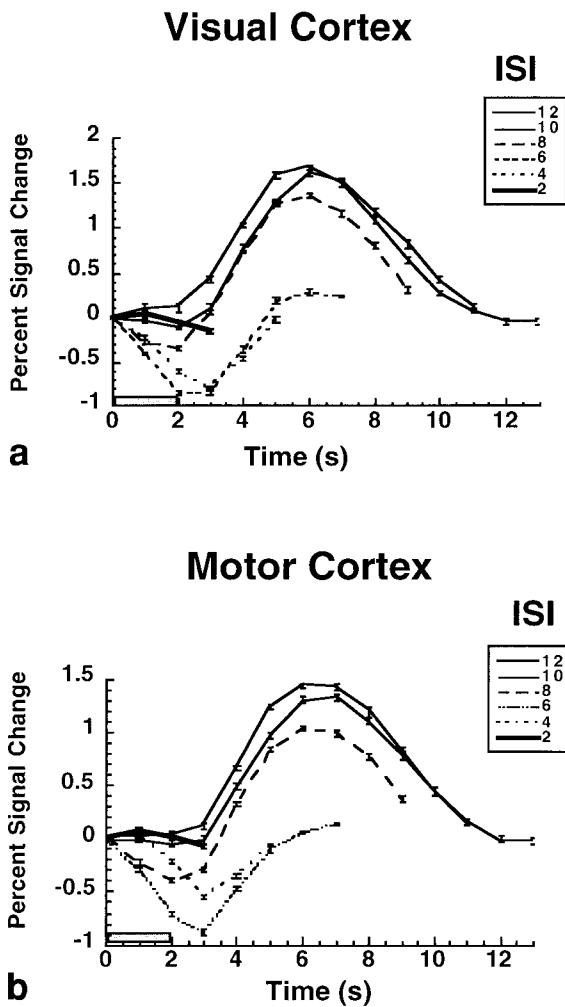
Visual Cortex

a

Motor Cortex

b

FIG. 4. Cycle-averaged time series from (**a**) visual and (**b**) motor cortex. The fractional signal change, relative to the time point collected at the start of each 2-sec activation, is shown. ISI range is 2 to 12 sec. At ISIs of 8 sec and below, the apparent pre-undershoot is due to successive activation during the falling stage of the previous hemodynamic response. (Error bars are SEMs.)

time series, all successive on/off cycles were averaged. The cyclic-averaged time series, obtained from the raw time series shown in Fig. 3, are plotted in Fig. 4. The fractional signal change is shown in this display. At ISIs of 8 sec and below, the averaged time series shows what appears to be a pre-undershoot. This pseudo-pre-undershoot is because the ISI was less than the time for the hemodynamic response to fully return to baseline; therefore, the successive stimulus was given during the falling stage of the previous hemodynamic response. Figure 5 shows averaged time series from the set that used longer ISIs. The response function settles into a stable pattern above an ISI of about 8 sec.

Figure 6 shows contrast-to-noise images containing visual and motor cortex of two subjects. The same scale was used for all images. The contrast-to-noise decreases significantly below an ISI of 6 sec. The images obtained at ISI of 8 to 12 sec look qualitatively similar to those obtained using the blocked design. Figure 7 demonstrates that when

the contrast and intensity of the images are scaled up, activation is apparent even in the 2 sec on/2 sec off. Note that the regions of highest contrast-to-noise differ slightly between the blocked (ISI, SD = 20,20) and event-related (ISI,SD = 2,2) series types. This is particularly apparent in the visual cortex activation images, and may reflect differential responsivity across specific regions and/or vasculature structures of the brain.

A matrix of synthesized fMRI time series was created by convolution of a set of systematically varied boxcar neuronal input functions with the gamma-variate hemodynamic response used in the Theory section. The input ISI and SD were varied, at 1-sec intervals, from 1 to 32 sec. Figure 8a and b, respectively, shows the simulated "raw" responses and responses obtained after the response pattern reached a steady state using the same timing as used experimentally. These time series show an extremely similar shape and latency to those obtained in the data. In fact, the differences in time series within the data are considerably greater than the differences between these experimental and simulated time series. Figure 9 shows the resulting functional contrast matrix, calculated in the same manner as the functional contrast from the experimental time series plots. As in the Theory section, we see that the highest contrast results from balancing ISI and SD.

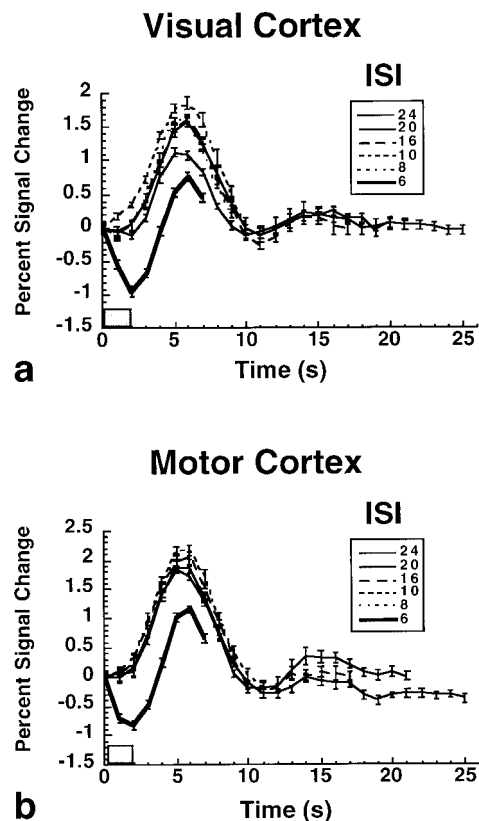Experimental and simulated results are summarized and compared in Fig. 10, which shows the single-event con-

Visual Cortex

a

Motor Cortex

b

FIG. 5. Cycle-averaged time series from (**a**) visual and (**b**) motor cortex. The fractional signal change is shown. ISI range is 8 to 20 sec. The response function settles into a stable pattern above an ISI of about 8 sec.
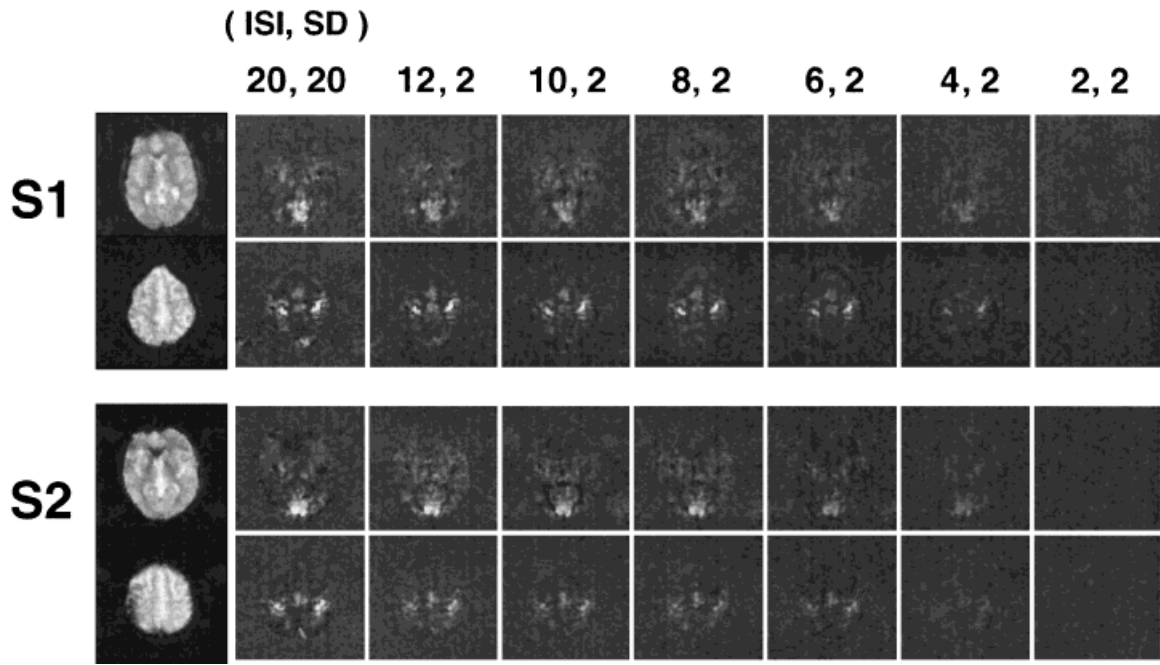
FIG. 6. Functional contrast-to-noise images from visual and motor cortex of two subjects. The same grayscale range was used for all images. The contrast-to-noise decreases rapidly below ISIs of 6 to 8 sec. The functional contrasts at ISIs of 8 to 12 sec appear qualitatively similar to those of the blocked-design time series.

trast per unit time normalized to the contrast obtained during the block design time series. The optimal experimental ISI for a 2-sec SD is about 12 sec. At the optimal ISI, the experimental contrast per unit time is only 35% lower than that of blocked-design paradigms. This is remarkable
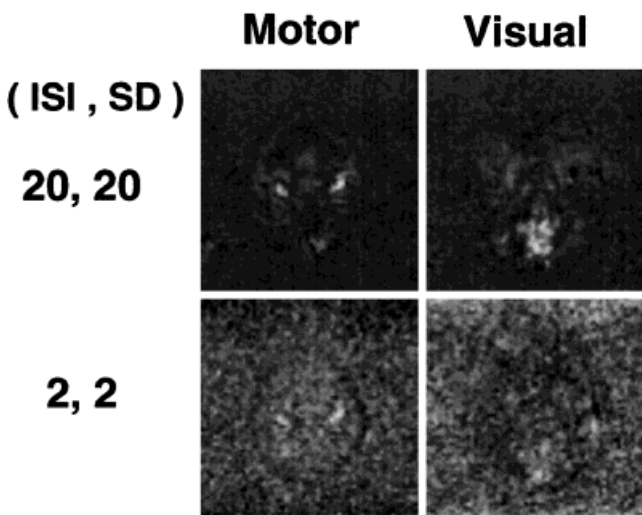

FIG. 7. Comparison of activated regions from the blocked and the event-related ISI = 2 sec paradigm, each image shown with a separate intensity-to-grayscale mapping chosen to enhance the visual contrast of the results. The scaled-up single-event contrast-to-noise image demonstrates that an alternating 2-sec-on/2-sec-off paradigm can be used to create a functional image, but the contrast is barely above the noise. Also, the regions of high contrast-to-noise differ slightly, suggesting differential responsivity to rapidly alternating stimuli across voxels within an activated region.
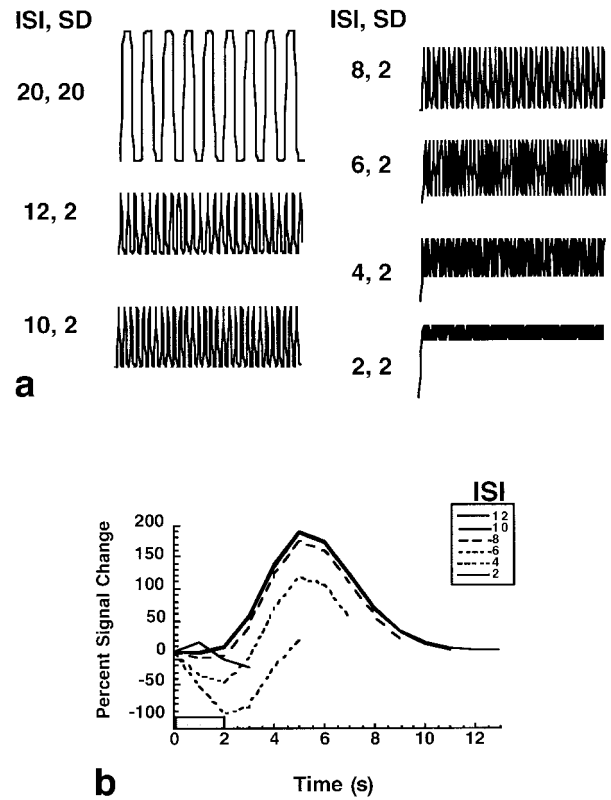

FIG. 8. Synthesized (**a**) raw responses and (**b**) responses obtained after the response pattern reached a steady state. Each simulated time series was created by convolution of a boxcar input function with the gamma-variate hemodynamic function described in the Theory section. The raw responses were created by convolution of a boxcar function representing the neuronal input.
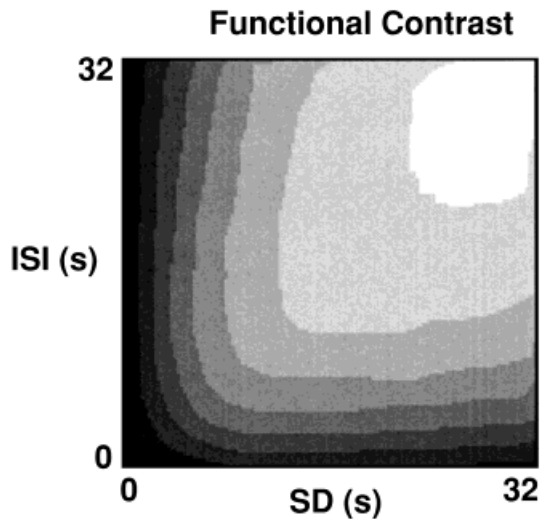
Functional Contrast

FIG. 9. A 32 × 32 matrix of synthesized functional contrasts. The functional contrasts were calculated from the simulated time series plots in the same manner as the experimental time series plots. The input ISI and SD were each varied, at 1-sec intervals, from 1 to 32 sec. All time series were created in the same manner as in Fig. 8.

because with blocked-design studies, the stimulus is "on" about half the time, and with this single-event timing, the stimulus is "on" only 14% of the time.

A projection through the surface in Fig. 9 along SD = 2 sec, shown as the dotted line in Fig. 10, reveals a contrast curve shape that is similar to the experimental contrast curve shape. The optimal simulated ISI is similar to that predicted theoretically but slightly shorter than that dem-
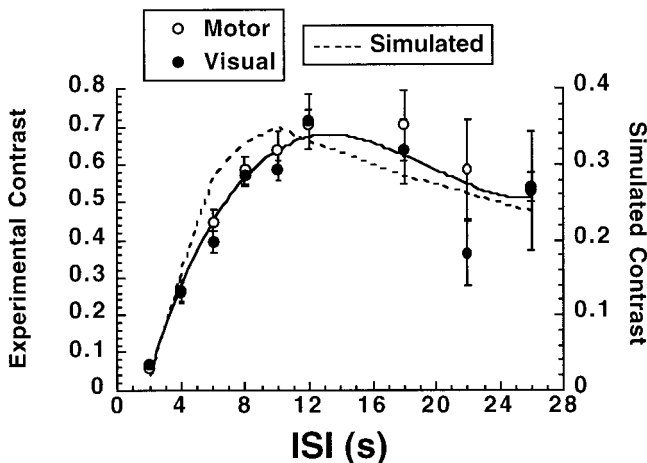

FIG. 10. Synthesized and experimental single-event contrast per unit time versus ISI. Contrast is normalized to the contrast obtained during the blocked-design time series (blocked-design contrast = 1). The experimental optimal ISI for a 2-sec SD is about 12 sec. At the optimal ISI, the experimental contrast per unit time is only 35% lower than that of a blocked-design paradigm. The synthesized optimal ISI for a 2-sec SD is about 10 sec. At the optimal ISI, the synthesized contrast per unit time is 65% lower than that of a blocked-design paradigm.

onstrated experimentally. This difference is likely due to minor differences in gamma-variate parameters used that would best fit the experimental data presented. While a change of the gamma-variate parameters can alter the peak response time, it does not alter the maximum contrast obtained relative to the calculated block design, since the function is linear. Another possibility is that the post-stimulus undershoot, not considered in the gamma-variate hemodynamic response model, could lengthen the optimal ISI slightly.

The functional contrast per unit time for the synthesized response is about 70% lower than that of blocked-design time series. This difference in contrast (but not optimal ISI) between the experimental results and the simulations suggests that the amplitude of the ER-fMRI data, relative to steady-state amplitude during a sustained stimuli, is larger than the relative amplitude of the synthesized response. This is in agreement with the results of Boynton et al. (12) and Vazquez and Noll (15), which suggested that one of the only aspects of the hemodynamic response that deviated from linearity was the amplitude of the response arising from brief stimulus durations. These results are not necessarily contrary to the results of Dale and Buckner (14) because, after a brief stimulus duration, the responses to successive brief stimuli may add linearly. It is only the initial amplitude of the first brief stimulus that is greater than that predicted in a linear system.

CONCLUSIONS

An analytic expression for the optimal constant ISI has been derived. This result has been confirmed experimentally using ER-fMRI time series of primary visual stimuli and motor tasks with varying ISI. The theoretically optimal ISI, given the gamma-variate function of Cohen (28) is 10.3 sec for a SD of 2 sec. As shown in Fig. 8, the experimentally derived optimal ISI, for an SD of 2 sec, is about 12 sec. The contrast-per-unit-time versus ISI curve is much steeper for shorter-than-optimal ISIs than for longer-than-optimal ISIs. It is therefore it is much less costly, from a contrast-to-noise standpoint, to err on the long ISI side.

The use of a constant ISI is only a special (and likely suboptimal) category of ER-fMRI paradigms. Previous work has demonstrated that randomization of ISI in a single time series, used in combination with deconvolution techniques, is likely to allow for a shorter average ISI with improved functional contrast (14,31,42,43). While these randomized ISI ER-fMRI techniques represent a substantial improvement in fMRI methodology for mapping regions of activation, accurate interpretation of derived results (i.e., absolute response magnitudes) requires the assumption that the event-related response behaves in a linear manner. Calculation of the optimal average ISI in the case where the ISI is randomized in the time series is the subject of ongoing research in this laboratory, but is beyond the scope of this paper. Preliminary work suggests that with deconvolution techniques and ISI randomization, optimal functional contrast is obtained by having an on/off distribution of 50%/50%, and that the ISI can be as short as desired, within the constraints of subject response times.

It has been found that with constant ISI, the experimental functional contrast per unit time was only 35% less than that

obtained with a blocked 20-sec-on/20-sec-off paradigm. While the optimal ISI was similar, this experimental ER-fMRI contrast was much larger than a synthesized time series using convolution of a gamma-variate hemodynamic "impulse response" with a boxcar neuronal input function. At the optimal ISI, the functional contrast of the synthesized response was about 65% less than that of a blocked-design paradigm. An important point to consider is that regardless of the specific parameters of the gamma function, the contrast obtained when using a linear contrast function is linearly proportional to the fraction of time that the stimulus is on. Therefore, the specific parameters chosen for the gamma function do not change these conclusions.

This difference in functional contrast is likely due to the fact that the experimental ER-fMRI amplitude, relative to steady-state "on" amplitude, is greater than that of the relative response created by linear convolution. Also, the post-stimulus undershoot, not considered in the gamma-variate hemodynamic response model, may enhance the functional contrast slightly. It is important to note that these results are from averaged ROIs in the visual and motor cortex, and may vary significantly across voxels within and between activated brain regions.

Reasons for nonlinearities in the event-related response can be neuronal, hemodynamic, and/or metabolic in nature. The neuronal input may not be a simple boxcar function. Instead, an increased neuronal firing rate at the onset of stimulation (neuronal "bursting") may cause a slightly larger amount of vasodilation that later reaches a plateau at a lower steady-state level. The amount of neuronal bursting necessary to significantly change the hemodynamic response, assuming a linear neuronal-hemodynamic coupling, is quite large. For example, to account for the almost double functional contrast for the experimental relative to the linear convolution-derived single-event responses, the integrated neuronal response over 2 sec must double. Assuming that neuronal firing is only at a higher rate for about the first 50 msec of brain activation, the neuronal firing rate must be 40 times greater than steady state for this duration.

BOLD contrast is highly sensitive to the interplay of blood flow, blood volume, and oxidative metabolic rate. If, on activation, any one of these variables changes with a different time constant, the fMRI signal may show fluctuations until a steady state is reached (44–46). For instance, an increase in blood volume would slightly reduce the fMRI signal because more deoxyhemoglobin would be present. If the time constant for blood volume changes were slightly longer than that of flow changes, then the activation-induced fMRI signal would first increase and then be reduced as blood volume later increased. Mandeville et al. (47) have demonstrated in rats that during forepaw stimulation, cerebral blood volume changes are slower than BOLD signal changes.

The same BOLD effect would be obtained if the time constant of oxidative metabolic rate were slightly slower than that of flow and volume changes. Evidence for increased oxidative metabolic rate after 2 min of activation is given by Frahm et al. (44), but no evidence is given to suggest that the time constant of the increase in oxidative metabolic rate is only seconds longer than the flow increase time constant, as would be required to be applicable only to relatively high-amplitude single-event responses. These hemodynamics, which may also differ on a voxel-wise basis, remain to be fully characterized. In addition, differences in the degree of neuronal activation, "bursting," and neuronal habituation may exist between higher order and primary brain activation, causing differences in the measured response parameters between cognitive and primary activation even for durations as short as 2 sec.

In this work, the optimal ISI for a constant ISI strategy has been experimentally demonstrated and theoretically derived. While use of a constant ISI for ER-fMRI may be preferable only in specific types of cognitive studies, information derived from these studies reveals nonlinearities in the hemodynamic response. These nonlinearities may pose a limitation in the precise interpretation of results obtained by linear deconvolution of a random stimulus input from the evoked hemodynamic responses.

Future work in event-related experimental optimization relies on what further information can be derived from these responses and in methods to work around nonlinearities. Between-region, between-voxel, between-subject, and stimulus-dependent variations in amplitude, latency, shape, and responsivity of the ER-fMRI signal remain uncharacterized. Furthermore, neuronal-physiologic mechanisms underlying these characteristics remain unclear. Work directed at clarifying the aspects of the ER-fMRI signal as well as the underlying mechanisms of the signal will certainly result in substantial increases in the overall utility of fMRI.

APPENDIX

Mathematical Notation

SD, stimulus duration. ISI, interstimulus interval; time from end of one stimulus to start of the next. T, repetition interval (SD + ISI). Δt, sampling interval (= TR in single-shot imaging). $r(t)$, ideal response function to a single stimulus occurring at time $t = 0$. $x(t)$, voxel response function. α, amplitude of $r(t)$ in voxel response function. β, baseline value of $x(t)$. ς, noise time series. σ^2, variance of noise. L, number of samples in repetition interval (= $T/\Delta t$). M, number of stimuli in an experiment. N, number of time series samples in an experiment (= LM). n, sample index, from 0 to $N-1$. $r^{(L)}$, N-vector giving summed ideal response to a train of stimuli. e_N, N-vector of all ones. P, $N \times 2$ matrix in Eq. [1c] = operator that maps unknowns (α, β) to voxel response vector x. x, sampled voxel response N-vector. μ_q, $\int_0^\infty r(t)^q dt$ for $q = 1,2$. T_{opt}, "optimal" repetition interval. b,c, parameters of the gamma-variate response, Eq. [6]. FWHM, full width at half maximum (of a response function).

REFERENCES

1. Bandettini PA, Wong EC. Magnetic resonance imaging of human brain function: principles, practicalities, and possibilities. Neurosurg Clin N Am 1997;8:345–371.

2. Bandettini PA, Wong EC, Hinks RS, Tikofsky RS, Hyde JS. Time course EPI of human brain function during task activation. Magn Reson Med 1992;25:390–397.

3. Belliveau JW, Kennedy DN, McKinstry RC, Buchbinder BR, Weisskoff RM, Cohen MS, Vevea JM, Brady TJ, Rosen BR. Functional mapping of the human visual cortex by magnetic resonance imaging. Science 1991; 254:716–719.

4. Ogawa S, Tank DW, Menon R, Ellermann JM, Kim S-G, Merkle H, Ugurbil K. Intrinsic signal changes accompanying sensory stimulation: functional brain mapping with magnetic resonance imaging. Proc Natl Acad Sci USA 1992;89:5951–5955.

5. Kwong KK, Belliveau JW, Chesler DA, Goldberg IE, Weisskoff RM, Poncelet BP, Kennedy DN, Hoppel BE, Cohen MS, Turner R, Cheng HM, Brady TJ, Rosen BR. Dynamic magnetic resonance imaging of human brain activity during primary sensory stimulation. Proc Natl Acad Sci USA 1992;89:5675–5679.

6. Ogawa S, Lee TM, Kay AR, Tank DW, Brain magnetic resonance imaging with contrast dependent on blood oxygenation. Proc Natl Acad Sci USA 1990;87:9868–9872.

7. DeYoe EA, Bandettini P, Neitz J, Miller D, Winans P. Functional magnetic resonance imaging (FMRI) of the human brain. J Neurosci Methods 1994;54:171–187.

8. Fransson P, Kruger G, Merboldt K-D, Frahm J. Temporal characteristics of oxygenation-sensitive responses to visual activation in humans. Magn Reson Med 1998;39:912–919.

9. Bandettini PA, Wong EC, Binder JR, Rao SM, Jesmanowicz A, Aaron EA, Lowry TF, Forster HV, Hinks RS, Hyde JS. In: LeBihan, editor. Diffusion and perfusion: magnetic resonance imaging. New York: Raven Press; 1995. p 335–349.

10. Friston KJ, Jezzard P, Turner R. Analysis of functional MRI time-series. Hum Brain Mapp 1994;2:69–78.

11. Cohen JD, Perlstein WM, Braver TS, Nystrom LE, Noll DC, Jonides J, Smith EE. Temporal dynamics of brain activation during a working memory task. Nature 1997;386:604–607.

12. Boynton GM, Engel SA, Glover GH, Heeger DJ. Linear systems analysis of functional magnetic resonance imaging in human V1. J Neurosci 1996;16:4207–4221.

13. Friston KJ, Josephs O, Rees G, Turner R. Nonlinear event-related responses in fMRI. Magn Reson Med 1998;39:41–52.

14. Dale AM, Buckner RL. Selective averaging of rapidly presented individual trials using fMRI. Hum Brain Mapp 1997;5:329–340.

15. Vazquez AL, Noll DC. Nonlinear aspects of the BOLD response in functional MRI. Neuroimage 1998;7:108–118.

16. Bandettini PA, Wong EC, DeYoe EA, Binder JR, Rao SM, Birzer D, Estkowski LD, Jesmanowicz A, Hinks RS, Hyde JS. The functional dynamics of blood oxygen level dependent contrast in the motor cortex. In: Proceedings of the SMRM 12th Annual Meeting, New York, 1993. p 1382.

17. Blamire AM, Ogawa S, Ugurbil K, Rothman D, McCarthy G, Ellermann JM, Hyder F, Rattner Z, Shulman RG. Dynamic mapping of the human visual cortex by high-speed magnetic resonance imaging. Proc Natl Acad Sci USA 1992;89:11069–11073.

18. Savoy RL, Bandettini PA, Weisskoff RM, Kwong KK, Davis TL, Baker JR, Weisskoff RM, Rosen BR. Pushing the temporal resolution of fMRI: studies of very brief visual stimuli, onset variablity and asynchrony, and stimulus-correlated changes in noise. In: Proceedings of the SMR 3rd Annual Meeting, Nice, 1995. p 450.

19. Savoy RL, O'Craven KM, Weisskoff RM, Davis TL, Baker J, Rosen B. Exploring the temporal boundaries of fMRI: measuring responses to very brief visual stimuli. In: Book of Abstracts, Society for Neuroscience 24th Annual Meeting, Miami, 1994. p 1264.

20. Hickok G, Love T, Swinney D, Wong EC, Buxton RB. Functional MR imaging during auditory word perception: a single-trial presentation paradigm. Brain Lang 1997;58:197–201.

21. Menon RS, Ogawa S, Hu X, Strupp JP, Anderson P, Ugurbil K. BOLD based functional MRI at 4 Tesla includes a capillary bed contribution: echo-planar imaging correlates with previous optical imaging using intrinsic signals. Magn Reson Med 1995;33:453–459.

22. Ernst T, Hennig J. Observation of a fast response in functional MR. Magn Reson Med 1994;32:146–149.

23. Hennig J, Janz C, Speck O, Ernst T. Functional spectroscopy of brain activation following a single light pulse: examinations of the mechanism of the fast initial response. Int J Imaging Syst Technol 1995;6:203–208.

24. Davis TL, Weisskoff RM, Kwong KK, Savoy R, Rosen BR. Susceptibility contrast undershoot is not matched by inflow contrast undershoot. In: Proceedings of the SMR 2nd Annual Meeting, San Francisco, 1994. p 435.

25. Stern CE, Kwong KK, Belliveau JW, Baker JR, Rosen BR. MR tracking of physiological mechanisms underlying brain activity. In: Proceedings of the SMRM 11th Annual Meeting, Berlin, 1992. p 1821.

26. Frahm J, Bruhn H, Merboldt K-D, Hanicke W, Math D. Dynamic MR imaging of human brain oxygenation during rest and photic stimulation. J Magn Reson Imaging 1992;2:501–505.

27. Buxton RB, Luh WM, Wong EC, Frank LR, Bandettini PA. Diffusion-weighting attenuates the BOLD signal change but not the post-stimulus undershoot. In: Proceedings of the ISMRM 6th Annual Meeting, Sydney, 1998. p 7.

28. Cohen MS. Parametric analysis of fMRI data using linear systems methods. Neuroimage 1997;6:93–103.

29. Josephs O, Turner R, Friston K. Event-related fMRI. Hum Brain Mapp 1997;5:243–248.

30. Buckner RL, Bandettini PA, O'Craven KM, Savoy RL, Petersen SE, Raichle ME, Rosen BR. Detection of cortical activation during averaged single trials of a cognitive task using functional magnetic resonance imaging. Proc Natl Acad Sci USA 1996;93:14878–14883.

31. Clark VP, Parasuraman R, Keil K, Kulansky R, Fannon S, Maisog JM, Ungerleider LG, Haxby JV. Selective attention to face identity and color studied with fMRI. Hum Brain Mapp 1997;5:293–297.

32. McCarthy G, Luby M, Gore J, Goldman-Rakic P. Infrequent events transiently activate human prefrontal and parietal cortex as measured by functional MRI. J Neurophysiol 1997;77:1630–1634.

33. Schacter DL, Buckner RL, Koutstaal W, Dale AM, Rosen BR. Late onset of anterior prefrontal activity during true and false recognition: an event-related fMRI study. Neuroimage 1997;6:259–269.

34. Zarahn E, Aguirre G, D'Esposito M. A trial-based experimental design for fMRI. Neuroimage 1997;6:122–138.

35. Birn RM, Bandettini PA, Cox RW, Shaker R. Event-related fMRI of tasks involving brief motion. Hum Brain Mapp 1999;7:106–114.

36. Birn RM, Bandettini PA, R. Cox RW, Shaker R. FMRI during stimulus correlated motion and overt subject responses using a single trial paradigm. In: Proceedings of the ISMRM 6th Annual Meeting, Sydney, 1998. p 159.

37. Bandettini PA, Cox RW. Contrast in single trial fMRI: interstimulus interval dependency and comparison with blocked strategies. In: Proceedings of the ISMRM 6th Annual Meeting, Sydney, 1998. p 161.

38. Cox RW, Bandettini PA. Single trial fMRI: the optimal inter-stimulus interval. In: Proceedings of the ISMRM 6th Annual Meeting, Sydney, 1998. p 244.

39. Bandettini PA, Cox RW. Functional contrast in event-related fMRI: interstimulus interval dependency and blocked design comparison. In: Proceedings of the 4th International Conference on Functional Mapping of the Human Brain, Montreal, 1998. p 552.

40. Wong EC, Bandettini PA, Hyde JS. Echo-planar imaging of the human brain using a three axis local gradient coil. In: Proceedings of the SMRM 11th Annual Meeting, Berlin, 1992. p 105.

41. Bandettini PA, Jesmanowicz A, Wong EC, Hyde JS. Processing strategies for time-course data sets in functional MRI of the human brain. Magn Reson Med 1993;30:161–173.

42. Buckner RL, Goodman J, Burock M, Rotte M, Koutstaal W, Schacter D, Rosen B, Dale AM. Functional-anatomic correlates of object priming in humans revealed by rapid presentation event-related fMRI. Neuron 1998;20:285–296.

43. Burock MA, Buckner RL, Dale AM. Understanding differential responses in event related fMRI through linear simulation. In: Proceedings of the ISMRM 6th Annual Meeting, Sydney, 1998. p 245.

44. Frahm J, Krüger G, Merboldt K-D, Kleinschmidt A. Dynamic uncoupling and recoupling of perfusion and oxidative metabolism during focal activation in man. Magn Reson Med 1996;35:143–148.

45. Buxton RB, Wong EC, Frank LR. Dynamics of blood flow and oxygenation changes during brain activation: the balloon model. Magn Reson Med 1998;39:855–864.

46. Menon RS, Ogawa S, Strupp JP, Anderson P, Ugurbil K. BOLD based functional MRI at 4 tesla includes a capillary bed contribution: echo-planar imaging correlates with previous optical imaging using intrinsic signals. Magn Reson Med 1995;33:453–459.

47. Mandeville JB, Marota JJ, Kosofsky BE, Keltner JR, Weissleder R, Rosen BR, Weisskoff RM. Dynamic functional imaging of relative cerebral blood volume during rat forepaw stimulation. Magn Reson Med 1998; 39:615–624.